Estimation of Rain and Hail Rates in Mixed-Phase Precipitation

N. BALAKRISHNAN* AND D. S. ZRNIĆ

NOAA, Environmental Research Laboratories, National Severe Storms Laboratory, Norman, Oklahoma

(Manuscript received 2 March 1989, in final form 25 August 1989)

ABSTRACT

Precipitation comprising rain and hail is studied. Specifically, techniques to identify and quantify such precipitation in terms of rain and hail fall rates using dual polarized radar data, are presented. Included for consideration are Z_H, the reflectivity factor for horizontal polarization, Z_{DR}, the differential reflectivity, and K_{DP}, the differential propagation constant. A variety of simple models of mixed-phase precipitation are first examined. Electromagnetic scattering computations are performed to simulate and study the behavior of Z_H, Z_{DR}, and K_{DP}. It is shown that it is possible to distinguish the mixed-phase precipitation from either rain or hail by using Z_H, K_{DP} pair and also to infer the thermodynamic phase and orientation from Z_H, Z_{DR} pair. On the basis of physical principles, it is shown that K_{DP} senses primarily liquid water in the form of raindrops even when these are mixed with hailstones. The self-consistency of Z_H, Z_{DR}, and K_{DP} is then exploited to estimate both the rain and hail fall rates. The ability of the methods to estimate rain and hail fall rates is demonstrated with actual radar data from two Oklahoma storms.

1. Introduction

A long-standing problem in meteorology is that of distinguishing, by remote probing radars, between ice and water phases of precipitation. This is especially challenging in convective storms, where water can exist at temperatures below 0°C and ice can be found at temperatures above 0°C. Virtually all single and multiparameter radar techniques conceived so far, have, at one time or another been aimed at this problem, (for instance, see Special Issue of *Radio Science,* Vol. 19, No. 1, Jan–Feb 1984). Equally important is the problem of quantifying rain- and hailfall rates when the precipitation is a mixture of the two.

A single static hydrometeor is characterized by two independent measurements of its major and minor axes, if simplifying and often justifiable assumptions are made, such as spheroidal shape of the scatterer and negligible effects due to the intervening medium, the differential phase shift upon scattering, and the canting angle. If an assembly of scatterers fills the resolution volume of the radar, as many pairs of independent measurables as the number of different categories of scatterers are needed to comprehensively solve the inverse scattering problem. This is technically not feasible and intractable. In such situations, often the recourse is taken to model the distribution of scatterer shapes, sizes, thermodynamic phase, and canting angles with known and physically plausible functional forms. The radar is then used to estimate a finite number of parameters of the assumed model. This is justified since the parameters of meteorological interest are the bulk properties like rain rate, hail rate, and liquid water content. Most common is the estimation of rain rate from the reflectivity factor wherein the rain drop size distribution is characterized by a single parameter. It should be pointed out here that, in reality, the scatterers are in motion, and this leads to fluctuations in radar signals that are due to random constructive and destructive interference among the backscattered waves from each scatterer. Hence, the radar estimates are obtained from time averages of autocorrelations and cross correlations of received echoes.

Polarization radars, as well as multiwavelength radars, permit the estimation of more than one independent variable. These additional measurements of precipitation echo characteristics can be used, in principle, to estimate parameters such as the mean values and the breadth of the distributions of size or shape, and spatial orientation of the particles filling the radar resolution volume, their thermodynamic phase, and also the bulk properties of the intervening medium. However, even with the most advanced radars, the available independent measurables are fewer than necessary to estimate all of these parameters. Hence, in most cases the radar observations are interpreted in the light of

* NRC Research Associate, on leave from Department of Aerospace Engineering, Indian Institute of Science, Bangalore-560012, India.

Corresponding author address: Dr. Dusan S. Zrnić, NOAA/ERL, National Severe Storms Laboratory, 1313 Halley Circle, Norman, OK 73069.

other experimental/theoretical evidence relating to size, shape, and spatial orientations of the hydrometeors. Even with such simplifying assumptions, the interpretation of backscatter data from a single resolution volume is difficult. This is because several precipitation models yield the same backscatter signatures; i.e., the inverse problem is not unique. Therefore, one must capitalize on the ability of the radar to scan a volume. This yields spatial profiles of polarization variables from which information about precipitation habitats and their thermodynamic phase could be obtained.

Polarimetric radar measurements and interpretations owe much of their development to the extensive theoretical and experimental work of McCormick and Hendry (1975, 1979). They were the first to measure relative phase and coherency of co- and cross-polar echoes. These measurements together with the circular depolarization ratio (CDR) led them to infer the extent of common alignment and oblateness of hydrometeors. Seliga and Bringi (1976) used the evidence that raindrop oblateness is related to size (Green 1975) and that the drops are highly oriented. On these bases, they showed that the two parameters of an assumed exponential size distribution can be estimated from the measured values of Z_{DR}, the differential reflectivity, and of Z_H, the reflectivity factor for horizontal polarization. Coherent radars that are capable of measuring Z_{DR} could also measure the two-way differential propagation constant K_{DP} that according to Seliga and Bringi (1978) may be used instead of Z_{DR} to estimate the drop size distribution. Both Z_{DR} and K_{DP} can be derived from circularly polarized echoes as suggested by McGuinnes and Holt (1989). This paper explores the possibility of discriminating between pure rain, pure hail, and rain and hail mixed-phase precipitation on the basis of radar measurements of Z_H, Z_{DR}, and K_{DP}; an attempt to quantify the contributions due to rain and hail is also made. Many of the earlier studies reported in the literature are confined to discriminating between pure rain and pure hail phases of the precipitation. Steinhorn and Zrnić (1988) explored methods to identify mixed-phase precipitation, but there have been no published results allowing quantification in terms of rain- and hailfall rates.

Of the three polarization measurables, Z_H and Z_{DR} are affected by both anisotropic (like rain) and isotropic (like spherical or tumbling hail) constituents of the precipitation. However, K_{DP} is independent of the isotropic constituents. Even anisotropic hail, containing oriented oblate spheroids, affects Z_{DR} and K_{DP} differently. Though both Z_{DR} and K_{DP}, in a sense, measure the oblateness of hydrometeors, K_{DP} is affected very little by the addition of hail. This is due to a lower number concentration associated with hailstones and their smaller dielectric constant, compared with that of raindrops. But because Z_{DR} is a measure of the reflectivity weighted oblateness (Jameson 1983), the hail part of the mixed-phase precipitation contributes dominantly to the measured Z_{DR}. These different attributes of Z_{DR}, Z_H, and K_{DP} are used in this paper as ideal tools for diagnosing mixed-phase precipitation. With the recent studies relating the linear and circular polarization measurements (Jameson 1987), it is also possible to use the techniques presented here for interpreting the measurements made with radars employing circular or slant linear polarizations.

We first establish that it is possible to identify (on the basis of Z_H and K_{DP}) and quantify (on the basis of Z_H, Z_{DR}, and K_{DP}) individual contributions due to rain and hail. This is based on the computations of scattering parameters from which the polarization observables are calculated. An important premise of the technique is the characterization of the hailstone size distribution by a single parameter. Although it is somewhat justified by earlier experimental evidence (Cheng and English 1983), this premise is the weakest link in the method and is needed to quantify the hail part of precipitation. Our technique is facilitated by the relative insensitivity of the rain rate obtained from K_{DP} to drop size distribution variations (Sachidananda and Zrnić 1987). Furthermore, if the thermodynamic phase (i.e., dry or wet) and orientation of the hailstones are known, Z_H and K_{DP} are sufficient to identify the mixed-phase precipitation and also estimate the rainfall and hailfall rates. Thus from the fall rates, it is possible to compute the Z_{DR}. In order to obtain the actual thermodynamic phase and orientation of hailstones, Z_H–K_{DP} measurements are used to estimate the rain- and hailfall rates and compute the Z_{DR} for a few realistic hail models. Phase discrimination is achieved by comparing the computed Z_{DR} values with the measured Z_{DR}. It is shown here that among the considered hailstone models there is only one characterizing the thermodynamic phase and orientation of hail for which the computed Z_{DR} (from Z_H–K_{DP} measurements) agrees well with the measured Z_{DR}. In essence, a self-consistent set of Z_H, Z_{DR}, and K_{DP} provides sufficient information for determining the individual contributions due to rain and hail, as well as the type (i.e., wet or dry) and orientation of hail. Actual radar observations of Z_H, Z_{DR}, and K_{DP} and their vertical profiles demonstrate that it is possible to identify rain and hail in mixed precipitation, and also quantify their individual fall rates.

2. Techniques for hail identification

In single-parameter radar studies, the ability of the radar to map the reflectivity profiles, over a volume, is exploited to infer the presence of hail. The vertical profiles of reflectivity, the maximum reflectivity, and the height of the 45-dBZ level above the 0°C isotherm are used, with some success, to define criteria for hail detection (Waldvogel et al. 1979). A 55 dBZ threshold on reflectivity is another useful indicator of the possible presence of hail (Mason 1971).

Dual-wavelength radars, in principle, attempt to identify hail from measurements of reflectivity at two wavelengths (Atlas and Ludlam 1961). Despite subsequent suggestions by Eccles and Atlas (1973) for the use of the range derivative of the ratio of echo powers received at 10- and 3-cm wavelengths, the dual-wavelength radars, in practice, have not provided evidence of consistent and reliable hail discrimination (Jameson and Srivastava 1978). Rinehart and Tuttle (1984) brought out the fact that serious errors are caused by mismatched antenna beams and the attenuation effects at shorter wavelength, rendering the reliable interpretation of dual-wavelength signals difficult. However, recent exercises of Tuttle et al. (1988) show promising applications of dual-wavelength observations combined with dual polarization, in the study of the evolution of intense storms. Yet, because of tight frequency allocation policies and a factor two increase in hardware, dual-wavelength radar is not a candidate for nationwide operational application.

Barge (1972), using a 10-cm circular polarization radar, measured the effective reflectivity factor Z_e, the circular depolarization ratio (CDR), and the phase between echoes received in orthogonal polarization channels. Comparing surface reports of precipitation type with the radar measurements overhead, he brought out that simultaneous measurements of Z_e and CDR provides a better indication of hail than either quantity alone. This is because Z_e and CDR values for pure rain and pure hail fall in distinctly different regions of the Z_e–CDR plane. His measurements also indicated that orthogonally polarized echoes from storms that produce hail have larger phase differences than echoes from storms with only rain. However, no conclusive quantitative evidence could be drawn because separation of differential propagation phase shifts from differential phase shifts due to scattering was not possible in these measurements.

Using linear polarized radar data, Leitao and Watson (1984) established a boundary in the Z_H–Z_{DR} space that separates rain from hail. Bringi et al. (1984) presented convincing evidence of hail detection with the Z_H, Z_{DR} pair measurement. These successes have prompted several studies devoted to exploring the Z_H and Z_{DR} combination, augmented with the information obtainable from vertical profiles of Z_H and Z_{DR}, to effectively discriminate between precipitation phases. Most notable are the extensive studies of Bringi et al. (1986a, 1986b) where a detailed graupel–hail melting model is coupled with the electromagnetic backscatter model to describe the vertical profiles of Z_{DR} and linear depolarization ratio LDR. They compared the theoretical results for the distribution of ice spheroids with radar measurements. Based on simulated radar data from disdrometer measurements, Aydin et al. (1986) proposed a new hail signal H_{DR}, a measure of departure of the observed Z_H from the hail–rain boundary in Z_H–Z_{DR} space. These studies, prima facie, established that the polarization radars are aptly suited for detection of, and discrimination between, ice and liquid phases of precipitation.

Though the techniques of utilizing the hail-rain boundary, either in the Z_e–CDR or Z_H–Z_{DR} space, and the vertical profiles measured by the radar, could be effective in discriminating between pure rain and pure hail states of the precipitation, they become ambiguous and less effective when the radar encounters mixed-phase precipitation. For instance, the large spread of Z_{DR} around a mean value, due to drop size distribution variations, makes it difficult to establish the boundary precisely. In reality, the boundary between the hail and rain phases is diffuse, being characterized by hydrometeor phases where rain and hail coexist. The presence of large nonrain hydrometeors, even in small amounts, if not inferred and accounted for, leads to large errors in the rain rates predicted using Z_H and Z_{DR}. It is imperative that the boundaries for discrimination between rain and hail should be based on appropriate polarization measurables such that the estimated rain-and hailfall rates are within acceptable accuracies even in mixed-phase precipitation region. It is shown in the following sections that the polarization measurables, Z_H and K_{DP}, are suited for this.

3. Dual linear polarization radar observables

A typical dual linear polarized radar alternately transmits vertically and horizontally polarized electromagnetic waves and receives polarized backscattered signals. Because the hydrometeors are not exactly spherical, their radar backscatter cross sections are not the same for the vertically and the horizontally polarized transmissions, nor are the propagation characteristics of the medium containing such hydrometeors.

a. Estimation of polarimetric parameters

Representing the complex (i.e., amplitude and phase) samples of echoes from a given resolution volume as H and V for horizontally and vertically polarized transmissions, respectively, we obtain the mean powers $\hat{P}_H$ and $\hat{P}_V$ by averaging M samples having the same polarization:

$$\hat{P}_H = \frac{1}{M}\sum_{n=1}^{M} |H_{2n}|^2, \tag{1}$$

$$\hat{P}_V = \frac{1}{M}\sum_{n=1}^{M} |V_{2n+1}|^2. \tag{2}$$

The differential reflectivity (Z_{DR}) is expressed in decibels as

$$Z_{DR} = 10 \log\left(\frac{\hat{P}_H}{\hat{P}_V}\right). \tag{3}$$

This definition based on a square law estimator of powers (1), (2) has been established as the best esti-

mator (Sirmans and Dooley 1986; Chandrasekar et al. 1986) with lowest variance for a given number of samples. The reflectivity data used here are averaged over at least 1 km in range and have standard errors less than 1 dB; similarly, standard errors in Z_{DR} are less than 0.1 dB.

Another measurable, specific to the dual polarized radar, is the differential propagation constant K_{DP}. In an anisotropic precipitation medium, propagation constants for the vertically and horizontally polarized signals are different. Thus, the vertically and the horizontally polarized signals backscattered from a resolution volume arrive at the receiver with different cumulative phase shifts. The phase difference ϕ_{DP} for the entire two-way propagation path can be extracted from the echo samples. Estimation of ϕ_{DP} requires more than measuring the phase difference between H and V signals, because the H and V transmissions are not simultaneous but alternate. This introduces an additional phase shift between H and V samples, due to Doppler shift. An estimator suggested by Mueller (1984) and Jameson and Mueller (1985) can extract ϕ_{DP} from alternately polarized waveforms. The estimator is given by

$$\phi_{DP} = \frac{1}{2} \arg[\hat{R}_a \hat{R}_b^*], \tag{4}$$

where $\hat{R}_a$ and $\hat{R}_b$ are autocorrelation estimates from M consecutive HV and VH pairs given by

$$\hat{R}_a = \frac{1}{M} \sum_{n=1}^{M} H_{2n}^* V_{2n+1}, \tag{5}$$

$$\hat{R}_b = \frac{1}{M} \sum_{n=1}^{M} V_{2n+1}^* H_{2n+2}. \tag{6}$$

This estimator and its performance have been analyzed by Sachidananda and Zrnić (1986, 1989) who also suggested how to obtain Doppler shift from alternating sequence. Because K_{DP} is the rate of change of ϕ_{DP} with range, we choose the slope of linear regression line through ϕ_{DP} data over successive range locations as a suitable estimator. Thus $\hat{K}_{DP}$ is given by

$$\hat{K}_{DP} = \frac{\sum_{i=1}^{N} (\phi_{DPi} - \hat{\phi}_{DP})(r_i - \hat{r})}{\sum (r_i - \hat{r})^2}, \tag{7}$$

where ϕ_{DPi} and r_i are the two-way differential phase shift and range. The "hat" ($\hat{}$) indicates estimates of the mean values, and N is the number of contiguous range locations over which the estimate is made. It is seen that a larger weight is placed on the difference in $\hat{K}_{DP}$ between ranges that are farther apart. The variance of $\hat{K}_{DP}$ is linearly related to the variance of the differential phase shift σ_ϕ^2 by

$$\text{var}(\hat{K}_{DP}) = \frac{\sigma_\phi^2}{\sum (r_i - \hat{r})^2}. \tag{8}$$

With 256 alternately polarized samples (i.e., $M = 128$), it is possible to limit the statistical uncertainties in ϕ_{DP} to less than 1.72° if Doppler spectrum widths are larger than 1 m s^{-1} and correlation coefficient between H and V echoes are larger than 0.98 (Fig. 2 in Sachidananda and Zrnić 1986). In all the results presented here, data over 2.25 km are considered for obtaining K_{DP}. This gives an accuracy better than 0.6 deg km^{-1}, that is, a 40% improvement over the estimator that takes a linear average to calculate K_{DP} with a same range resolution.

In order to verify the rain phase in Z_H–K_{DP} space and also the standard error in the radar estimates of K_{DP}, data from a storm on 10 June 1986 is analyzed. The data was collected with a 10 cm wavelength radar performing sector scans at a fixed elevation of 1 deg. The data analyzed are from 38 to 62 km with a range resolution of 150 m. Range and elevation angle are chosen as above to ensure that the data set is not unduly affected by ground clutter and also does not include echoes from resolution volumes near the melting layer. The radar configuration was such that a calibrated reflectivity factor Z was obtained in real time from a sum of Z_H (dBZ) and Z_V (dBZ). Thus, whenever data is presented the symbol Z signifies this average. In our calculations we use Z_H because it has a clear physical meaning, it differs only slightly from Z and in the future it will be available in real time.

A scatter plot of Z and K_{DP} pairs in rain, is given in Fig. 1. In this figure Z is averaged over 2.25 km, and Eq. (7) is used to calculate K_{DP} over the same distance. The mean of about 1400 Z–K_{DP} pairs in Fig. 1 is in excellent agreement with the Z–K_{DP} relationship

$$Z = 13.86 \log(K_{DP}) + 44 \tag{9a}$$

which is derived from the assumption of M–P drop size distribution. In Eq. (9a), Z is in dBZ and K_{DP} is in deg km^{-1}. The rms deviation from the mean of Z–K_{DP} pairs [Eq. (9a)] for the data in Fig. 1 (at constant Z) is found to be 0.72 deg km^{-1}. The difference between this error and the theoretical standard error of 0.63 deg km^{-1} [obtained from Eq. (8) for a measured correlation coefficient of 0.98] could be attributed to the variation in the drop size distribution.

A curve depicting the boundary of Z–K_{DP} scatter is included in Fig. 1. The empirical relationship for this boundary that distinguishes the pure rain from mixed-phase and hail is given by

$$Z = 8 \log(K_{DP}) + 49. \tag{9b}$$

Although hail did not fall on the ground it is not possible to explain unambiguously the few points above the boundary in Fig 1. Imperfections of the boundary and statistical uncertainty may be the cause, but presence of partially frozen precipitation aloft or some contamination with ground echoes can not be excluded.

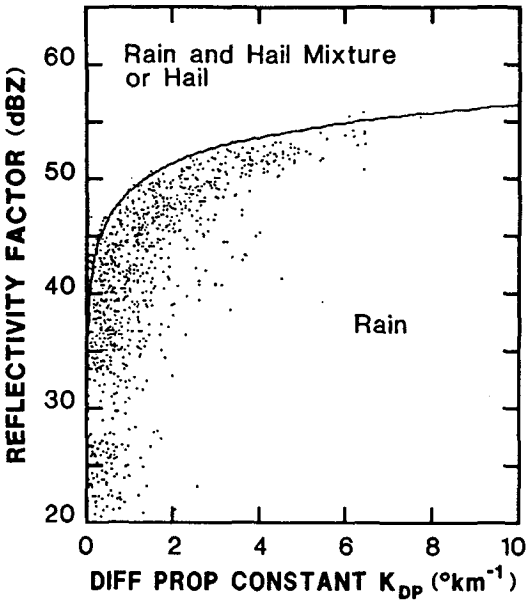

FIG. 1. Scatter plot of Z–K_{DP} of about 1400 radar measurements from a storm on 10 June 1986. Z is an average of reflectivity factors Z_H (horizontal polarization and in dBZ) and Z_V (vertical polarization).

The lower the measured K_{DP} from that given by Eq. (9b), the higher the probability that the precipitation contains hail. The analysis of data from another storm on 20 May 1985 yielded the same boundary as that given in Eq. (9b). It is worth noting that the curves (9a) and (9b) intersect at 55.6 dBZ. Experience suggests that when Z exceeds 55 dBZ hail is likely (Mason 1971); our data confirm and refine this heuristic criterion.

b. Relationships between Z_H, Z_{DR}, and K_{DP} in rain

In order to use Z_{DR} and K_{DP} for discriminating between hail and rain, it is necessary to understand the interrelationship between Z_H, K_{DP}, and Z_{DR} in rain and in hail. Compared with the hail medium, the rain medium is far simpler to characterize because raindrops, in general, are spheroidal and fall with their symmetry axes along the vertical. The mean axis ratios of the spheroidal rain drops is reasonably well approximated by the equilibrium model of Green (1975), which allows us to calculate Z_H, Z_{DR}, and K_{DP} from the drop size distribution (DSD). Although Z_{DR} and K_{DP} are differential parameters dependent on shape and size distribution, one interesting observation is that they have opposing tendency with variations in N_0, the intercept of the drop size distribution. Figure 2 shows a plot of Z_{DR} and K_{DP} variation, with N_0 for rain medium and Z_H as a parameter. With increasing N_0, Z_{DR} decreases, while K_{DP} increases, for a given Z_H. This is because Z_{DR} depends on N_0 only through the exponent Λ of the DSD [Eq. (10)], whereas K_{DP} depends explicitly on both N_0 and Λ. For a given Z_H, an increase in N_0 necessarily means a large number of smaller drops with smaller axis ratios. This reduces Z_{DR}. But, the total water content in the resolution volume becomes larger with increasing N_0; this increases the differential propagation constant at a higher rate than the reduction by a decrease in average axis ratios. In the following sections, the interrelationship between Z_H, Z_{DR}, and K_{DP} are analyzed in rain and hail mixtures.

4. Rain–hail models

Theoretical models used in the study of rain and hail are discussed in this section. The effect of the variations in hail–rain fraction in the mixture, and the type and orientation of hail, on Z_H, Z_{DR}, and K_{DP} is analyzed in detail.

a. Rain model

In practice there is no need to consider any specific drop size distribution because K_{DP} directly provides liquid water content and rain rate that are relatively insensitive to DSD variations (Sachidananda and Zrnić 1986). But for modeling purposes one must resort to a representative distribution. Therefore, the theoretical calculations presented here assume the well-known truncated Marshall-Palmer (MP) drop size distribution, which is given as

$$N(D) = N_0 e^{-\Lambda D}, \quad 0 \leq D \leq D_{\max}. \qquad (10)$$

The intercept parameter N_0 is constant and is equal to 8000 m^{-3} mm^{-1}. This form has the advantage that a single parameter Λ describes different raindrop size distributions. Green's equilibrium drop shape (Green 1975) is used, and the raindrops are assumed to be oriented with their minor axes vertical. The maximum diameter $D_{\max}$ is set at 7 mm, whereas the relationship between the terminal velocity and size is taken as given by Atlas and Ulbrich (1977). The radar wavelength is

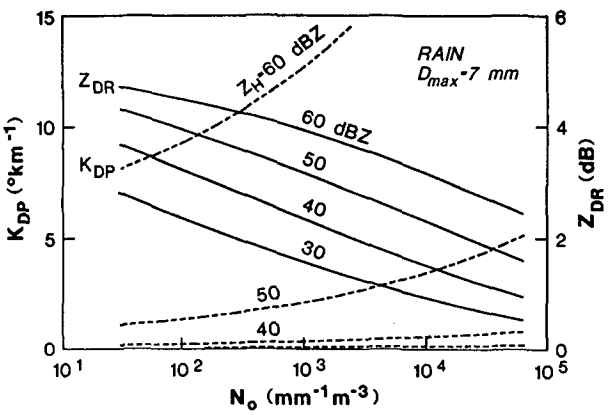

FIG. 2. Variations of Z_{DR} and K_{DP} in a pure rain medium with fixed Z_H.

10.4 cm, which justifies the choice of Rayleigh approximations for the scattering by raindrops.

b. Hail model

One of the inherent difficulties in inferring the physical properties of hail from radar measurement is the lack of adequate models with manageably few variable parameters that could describe the shape, size, orientation, and dielectric constant of hail. Generally the distribution of sizes is a three parameter distribution consisting of N_0, Λ, and D_{max}. Therefore, even when hail is remotely detected it is very difficult to determine the maximum size not to mention the other two parameters. The data collected on the numbers and sizes of hailstones, worldwide, indicate that reasonable approximations could be made about size (Douglas 1964; Ulbrich and Atlas 1982; Cheng and English 1983; Ziegler et al. 1983) and the shape (Barge and Isaac 1973; Torlaschi et al. 1984; Knight 1986), in order that the radar measurables are amenable to meaningful interpretation.

1) SIZE DISTRIBUTION OF HAIL

On the basis of samples collected at Alberta, Douglas (1964) suggested the use of exponential distribution to approximate the size distribution of hailstones. Ziegler et al. (1983) found that a gamma distribution is better suited. The observations of Carte and Held (1978) revealed that sometimes showers of large hail are nearly monodispersed. Cheng and English (1983) showed the usefulness of the following exponential model in describing the hail size distribution:

$$N(D) = N_0 \exp(-\Lambda D);$$

$$N_0 = 115\Lambda^{3.63}\ (\mathrm{m^{-3}\ mm^{-1}}), \qquad (11)$$

where Λ is in $\mathrm{mm^{-1}}$ and D is in mm. This affords the convenience of using a single parameter to describe the hail precipitation or hailfall rate R_h ($\mathrm{mm\ h^{-1}}$) that is related to Λ by (Torlaschi et al. 1984)

$$\Lambda = \left(\ln \frac{88}{R_h}\right) \Big/ 3.45. \qquad (12)$$

This distribution has also been used by other investigators (Torlaschi et al. 1984; Metcalf 1986; Bringi 1986a,b); hence the scattering computations presented here are also based on it. Thus whereas qualitative interpretation of the data based on this model is feasible quantitative inferences cannot be made with certainty. The maximum and minimum equivalent diameters are taken as 60.0 and 3.75 mm, respectively. Ulbrich and Atlas (1982) have shown that integral parameters such as reflectivity are insensitive to changes in the product ΛD_{max} for values of $\Lambda D_{max} > 5$. Thus our choice of large D_{max} is justified because the overwhelming majority of experimentally measured distributions have $\Lambda D_{max} > 5$ (Ulbrich and Atlas 1982). In preference to the empirical relationship given in Eq. (12), R_h is computed numerically. The fall velocities [$V(D) = 4.51 D^{0.5}$ m s^{-1}, D in mm] and densities are taken as those given by Cheng and English (1983).

2) SHAPE DISTRIBUTION OF HAIL

Barge and Isaac (1973) reported that 83% of the hailstones they observed had an axial ratio between 0.6 and 1.0, 15% between 0.4 and 0.6, and 2% less than 0.4 (Torlaschi et al. 1984). The analyses of hail shapes by Matson and Huggins (1980), Knight (1986), and several others also support the observation that the majority of hailstones are spheroidal and have an axis ratio of 0.8. Knight (1986) also observed that the Oklahoma hailstone embryos are predominantly frozen drops and are therefore nearly spherical. A few trial computations with the axial ratio distribution suggested by Barge and Isaac (1973) and also used by Metcalf (1986) did not produce results significantly different from those obtained by assuming a constant axial ratio of 0.8. Hence, ice and water-coated spheroidal hailstones are assumed to have an axial ratio of 0.8 as in Bringi et al. (1986b). In addition we consider spherical hail, which is also a good model for tumbling hail.

Although the constant axial ratio approximations are acceptable (Bringi et al. 1986b), Longtin et al. (1987) showed that, in the case of spongy ice, the backscatter properties are sensitive to axial ratio variations. This is particularly true when the water fraction is 30%–40%. The electromagnetic modeling described here also includes spongy hailstones with 40% water fraction for which the relationship between axial ratio and diameter is obtained from the measurements of Knight (1986).

3) ORIENTATION OF HAIL

List (1959) reported that 80% of hail in heavy hailfalls in Switzerland is ellipsoidal, and that these nonspherical stones fall with their minor axes vertical, thus acquiring a maximum drag coefficient and a minimum fall speed. On the basis of analysis of the structure of the hailstones, Knight and Knight (1970) contended that they fall with constant attitude sometimes and random tumbling at other times. Browning and Beimers (1967) observed that the growth structure of the hailstones could conceivably be produced by uniform fall with the minor axes vertical, whereas Knight and Knight (1970) observed that the minor axis wobbles considerably and is horizontal in the limit. Depending on the axis ratio, size of the spheroid, and the environmental damping, it is possible that one could observe either spherical (or isotropic if it tumbles) hail or oriented (anisotropic) hail (Pruppacher and Klett 1978). The anisotropic hail could be oriented with minor axes either vertical or horizontal. A randomly ori-

ented distribution of hydrometeors would statistically contribute to the dual polarization measurements, similar to spherical hydrometeors.

The horizontal reflectivity Z_H is more affected by changes in the phase of hydrometeors than by changes in their orientation or fall pattern for axial ratios of 0.8. Hence any effort to model hailstone orientation distribution using Gaussian or other functions is not likely to affect the variations of Z_H. Furthermore, because K_{DP} is very small in hail, the choice of model for hailstone orientation has no practical consequences. However, even in moderate hailfalls, the Z_{DR} of a mixture of rain and hail is completely dominated by the Z_{DR} of hail. Hence, the measured Z_{DR} could provide the necessary information concerning the orientation of hail. These arguments have led us to analyze the following cases: 1) all spheroids oriented with their minor axes vertical, 2) all spheroids oriented with their minor axes horizontal, and 3) all hailstones distributed with random orientations leading to a statistically isotropic medium.

4) Refractive indices and scattering coefficients of hail

Hailstones have been observed to have a wide variety of composition, depending on growth and environmental conditions. However, it is intuitive that spongy hailstones would have scattering properties that are close to those of pure ice (if the percentage of ice is very high) or pure water (if the percentage of water is high). Both of these can be calculated accurately. The vertical profile of Z_H and the height of the freezing level are useful in distinguishing between wet and dry hailstones. Also, estimates of liquid water content and hailfall rate are not affected significantly by the lack of information on the precise amount of liquid water within a hailstone. Hence, the results we present consider only pure ice, pure water, or spongy ice with 40% water fraction as constituents of hail. This particular percentage was chosen because it produces scattering properties that appear to differ most from those of wet and dry hail.

The refractive indices of water and ice are taken as $(9.0585 + 1.3421j)$ and $(1.78 + 0.007j)$ at a frequency of 2.88 GHz (Warner 1978). The refractive index of spongy hailstones is obtained from the refractive index formula for mixtures given in Longtin et al. (1987). The water fraction in the mixture is taken as 40%. The scattering coefficients for spheroidal hail are obtained from Warner (1978). Those for spherical and spongy hail are computed using a computer code for the extended T-matrix technique (Barber and Yeh 1975).

The scattering coefficients are used to compute the scattering cross sections. For reflectivity computations from the scattering cross sections, we assume the refractive index of water, irrespective of the thermodynamic phase of the precipitation, because that is a standard procedure in weather radars. The density of the ice part of hail is taken as 0.9 g cm^{-3}.

5. Polarization parameters for mixtures of rain and hail

a. Complete model

The results of the calculations of Z_H, Z_{DR}, and K_{DP} for various rain–hail mixtures presented here are based on the extended T-matrix method. The mixtures are characterized by the parameter ξ defined as

$$\xi = \frac{R_h}{(R_r + R_h)} = \frac{R_h}{R_e}, \tag{13}$$

where R_h, R_r, and R_e are the hail, rain, and equivalent precipitation rates in mm h^{-1}. Rainfall rates R_r up to 200 mm h^{-1} and hailfall rates R_h up to 60 mm h^{-1} are considered.

As explained earlier, the hail part of the mixed-phase precipitation spans:

1) spheroidal (anisotropic) hail oriented with minor axes either vertical or horizontal in the plane of polarization, axial ratio 0.8
2) spherical (isotropic) hail, and
3) spongy hail with 40% water function; axial ratio to diameter relationship for this case is obtained from Knight (1986).

Refractive indices of pure water and pure ice are assumed for wet and dry hail, respectively.

The variations of Z_H, and equivalent precipitation rate ($R_e = R_h + R_r$) with the hail fraction ξ as a parameter are shown in Fig. 3 for wet, dry, and spongy hail. The fact that wet hail has higher reflectivity than dry hail is often used to infer the thermodynamic phase of the precipitation from the vertical profile of Z_H. When the orientation of the minor axes of hail changes from vertical to horizontal, the horizontal reflectivity Z_H reduces by an amount equal to Z_{DR} as depicted by dotted lines in Fig. 3. Z_{DR} is dependent on orientation of hailstones and their thermodynamic state. It is about 1 dB for dry hail, and is greater than 2 dB for wet hail, and is zero for spherical hail. Because the axial ratio of our hail is 0.8, the reflectivity factors for spherical hail and oblate spheroidal hail are not significantly different. This shows that Z_H is more sensitive to the thermodynamic state of the hail (i.e., wet or dry) than to the orientation or the distribution of canting angles.

Constant Z_H and K_{DP} contours on the R_r–R_h plane, for wet, dry, and spongy hail are presented in Figs. 4. It can be inferred from the straight portions of curves that, even at moderate hailfall, Z_H is dominated by hail rather than by rain. An exactly opposite effect is seen in the contours of constant K_{DP}. Even in the heaviest wet hailfalls, changes in K_{DP} due to hail contamination are less than 1.3° km^{-1}. Furthermore K_{DP}

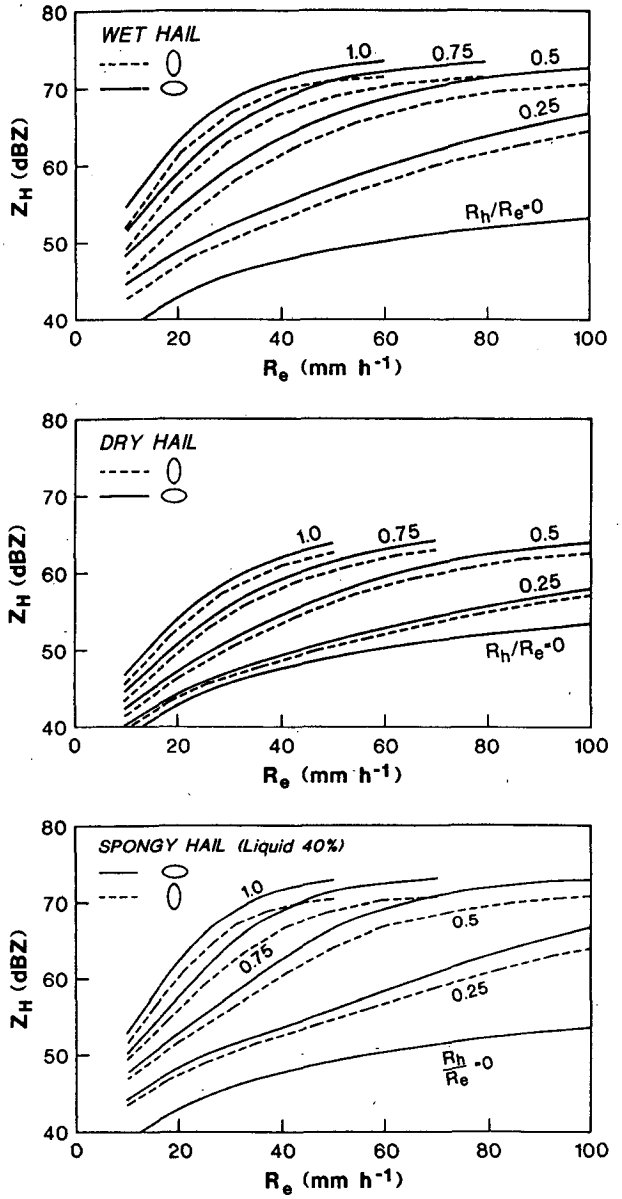

FIG. 3. Variations of Z_H with equivalent rain rate R_e (a) in mixtures of rain and wet hail. Orientation of hailstones is graphically indicated. (b) As in (a) but for dry oblate hail. (c) As in (a) but for spongy hail with 40% water.

is much less for dry hail, and zero for spherical hail. These attributes are reflected in the fact that constant Z_H and constant K_{DP} contours intersect at near right angles in the R_h–R_r plane. It is worth noting that the constant K_{DP} contours for spherical hail would be vertical lines in Fig. 4. The constant Z_H plots for spherical hail are nearly the same as those for spheroidal hail, and hence are not shown.

The interrelationships between Z_H and K_{DP} for various rain–hail mixtures are shown in Fig. 5. The hail has a lower N_0, near-spherical shape, and larger diameter, and dry hail has a lower dielectric factor. Addition of larger hailstones to the rain medium produces rapid increase in Z_H (dependence for small hailstones proportional roughly to D^6). The K_{DP} changes only if the oblate hailstones are oriented, and that too at a rate less than $D^{4.24}$ (Sachidananda and Zrnić 1986). These factors result, as seen in Fig. 5, in large, distinguishable deviations of Z_H–K_{DP} values in mixed phase from those in pure rain. In brief, the Z_H–K_{DP} values are more stable indicators of the mixed-phase precipitation than Z_H–Z_{DR}. This is particularly true when K_{DP} is higher than 0.5° km^{-1} (or rain rate larger than 10 mm h^{-1}).

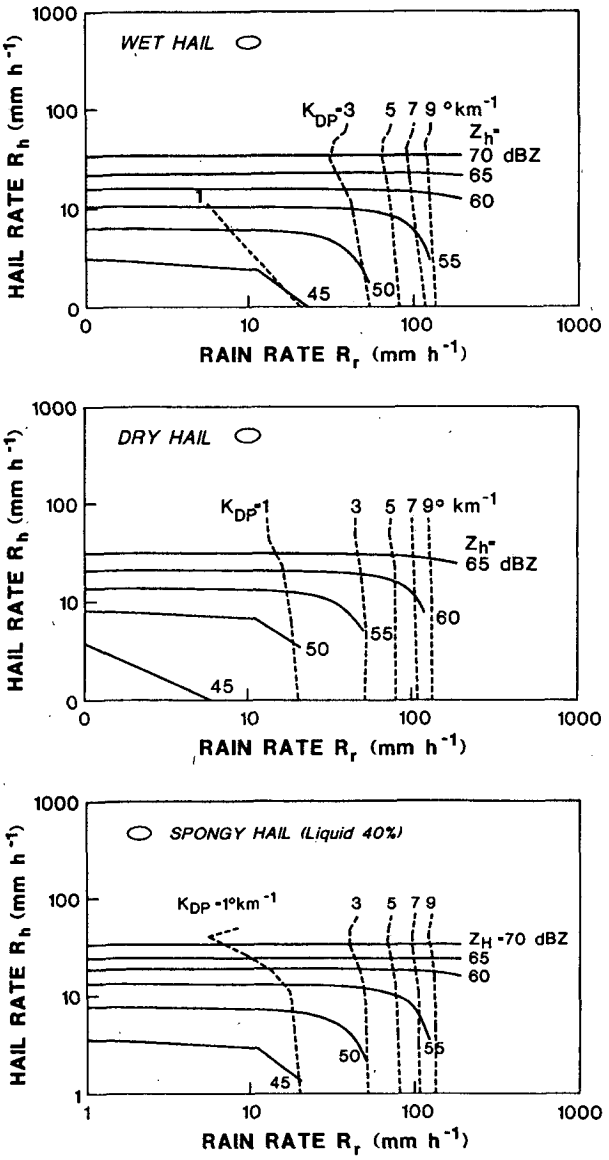

FIG. 4. Relationships among Z_H, K_{DP}, R_r, and R_h for (a) wet hail and rain mixtures. (b) As in (a) but for dry hail and rain mixtures. (c) As in (a) but for spongy hail and rain mixtures.

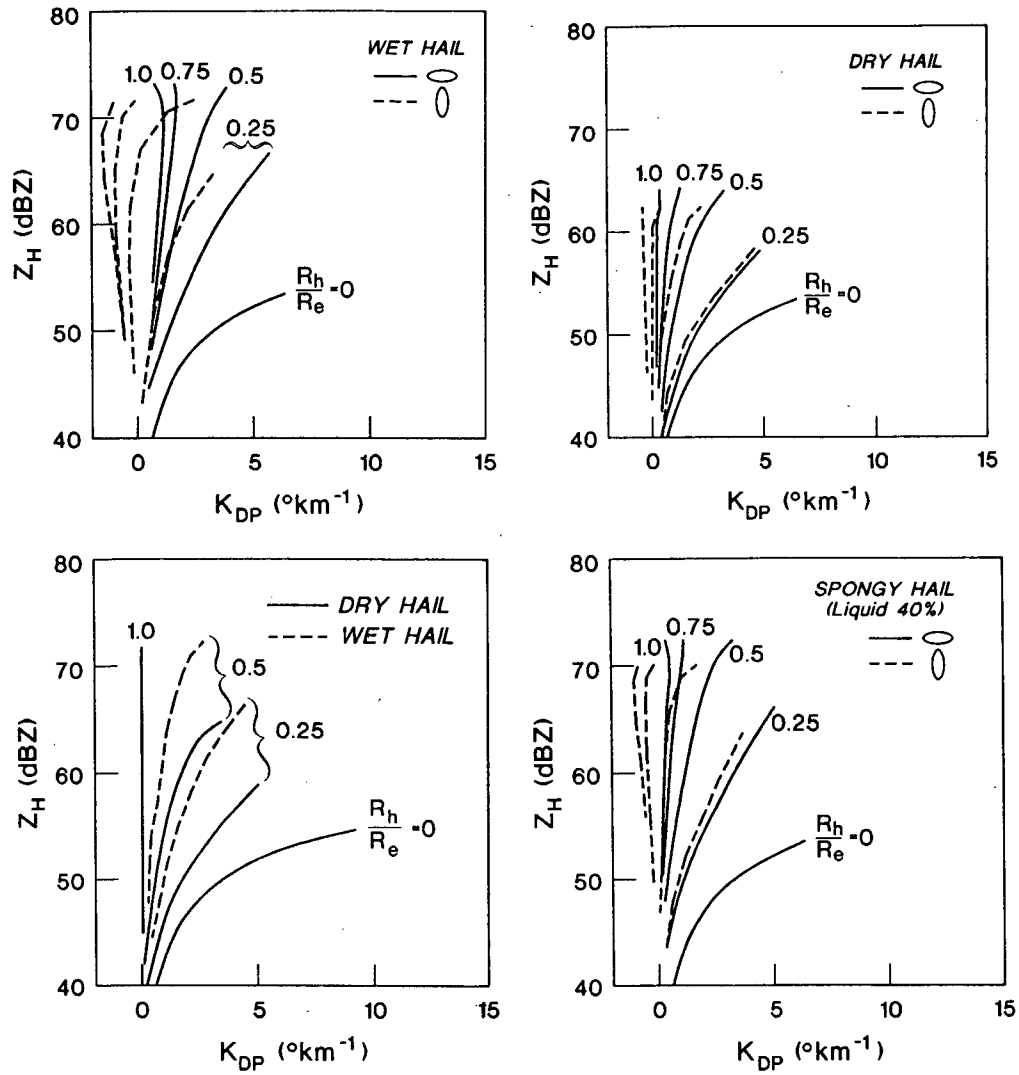

FIG. 5. Z_H–K_{DP} variations in (a) mixtures of rain and wet, oblate spheroidal hail. (b) As in (a) but for mixtures of rain and dry, oblate spheroidal hail. (c) As in (a) but for mixtures of rain and spherical hail. The curve for wet hail and $R_h/R_e = 1$ coincides with the curve for dry hail. (d) As in (a) but for a mixture of spongy hail and rain.

Figures 5a–d also indicate that, from the Z_H and K_{DP} pairs, it is possible to get the hail fraction ξ, and hence quantify individual contributions due to rain and hail, provided the information concerning the thermodynamic phase, orientation, and shape of hail is available. The shape and orientation information can be inferred from Z_{DR}. The inference can be verified by calculating the Z_{DR} for the appropriate model from Z_H and K_{DP}, (and hence ξ) and comparing it with the measured Z_{DR}. Model results in Fig. 3 to 5 are not sensitive to moderate changes in the maximum diameter, for hailfall rates that are less than 30 mm h^{-1}. For example, if D_{max} is reduced by a factor of 2 to 30 mm the reflectivity factor decreases by less than a dB. For hailfall rates of 50 mm h^{-1}, which is the maximum that we deduced in our data, the reduction is 6 dB. Thus the choice of 60 mm for D_{max} should not have a significant effect on the comparisons with our data, this however does not exonerate the use of Cheng and English distribution.

Shown in Fig. 6 are the Z_H–Z_{DR} plots for a few mixed-phase precipitation models. It is apparent that Z_{DR}, which is a measure of reflectivity weighted mean axis ratio (Jameson 1983; 1985), tends toward that of hail. The sign of Z_{DR} is solely influenced by the orientation of the minor axis in these models and is not very sensitive to the relative amount of rain. For spherical or tumbling hail Z_{DR} is close to zero. In spongy monodispersed hail Z_{DR} is known to vary between large positive and negative values with variations in diameter or axial ratio (Longtin et al. 1987). However, for exponential distribution (Cheng and English 1983) and

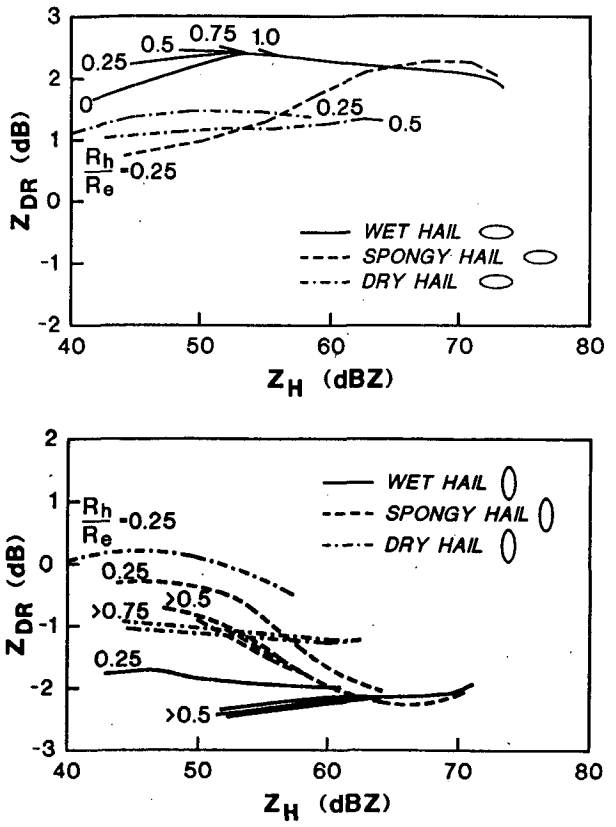

FIG. 6. Relationship between Z_H and Z_{DR} in (a) mixtures of rain and hail. (b) As in (a) but the orientation of the hailstones is with the minor axis horizontal.

axial ratio distribution given by Knight (1986), Fig. 6a shows that Z_{DR} is positive whenever the minor axis of the hail is oriented in the vertical. The Z_{DR} is negative (Fig. 6b) only when the minor axes are oriented in the horizontal direction. In essence, Z_{DR} is a good indicator of the orientation and shape of the hail part in a mixed phase.

It is seen from Fig. 6a that wet hail mixtures in the regions of 45–55 dBZ reflectivity yield Z_H–Z_{DR} measurements that are also possible in pure rain. This makes it difficult to identify mixed-phase precipitation on the basis of only Z_H–Z_{DR} measurements.

The discussions so far point out clearly that the measurement of Z_H, K_{DP}, and Z_{DR} can be used within admissible approximations to identify and quantify mixtures of rain and hail.

b. Simplified model

The scattering models analyzed earlier are applicable to isotropic and anisotropic hail. However, when the hail is isotropic, it is possible to quantify the hailfall and rainfall rates by using a simpler technique. Consider a homogeneous mixture of isotropic and anisotropic hydrometeors along a propagation path. Let the ensemble average of the propagation phase constant be $\langle k_V \rangle$ for vertical polarization and $\langle k_H \rangle$ for horizontal. Without loss of substance, attenuation can be neglected and these phase constants can be written as (Oguchi 1983).

$$\langle k_V \rangle = k_0 + \langle k_{Vr} + k_{Vh} \rangle, \tag{14a}$$

$$\langle k_H \rangle = k_0 + \langle k_{Hr} + k_{Hh} \rangle, \tag{14b}$$

where k_0 is the free-space propagation constant, k_{Vr} and k_{Vh} are contributions by rain and hail to the constant for vertically polarized waves, and k_{Hr} and k_{Hh} are similar contributions for horizontally polarized waves. Now for isotropic hail $\langle k_{Vh} \rangle = \langle k_{Hh} \rangle$, so after (14a) is subtracted from (14b) the two-way differential propagation constant becomes

$$K_{DP} = 2(\langle k_H \rangle - \langle k_V \rangle) = 2(\langle k_{Hr} \rangle - \langle k_{Vr} \rangle). \tag{15}$$

This remarkable yet simple result states that the differential propagation constant is affected by anisotropic hydrometeors only, (in this instance, rain). The physical explanation behind this fact is trivial. Isotropic hydrometeors produce equal phase shifts for either polarization, and the difference is due only to the nonisotropic constituents of the medium. Even for statistically isotropic hail mixed with rain, the K_{DP} will be mainly affected by rain drops if the water coating on hailstones is thin, mainly because ice has a considerably lower refractive index. In the next few paragraphs we briefly expose a method that allows separation of hail and rain contributions to the reflectivity factor.

To obtain the portion of reflectivity factor due to hail one needs to subtract from the measured Z the part produced by rain, Z_r. A direct estimate of Z_r is not available, but an indirect one may be obtained from the K_{DP}, R and Z_r, R relationships. For a wide range of drop size distributions a single $R(K_{DP})$ relationship gives accurate rain rate estimates. We use the relationship proposed by Sachidananda and Zrnić (1987):

$$R(K_{DP}) = 20.35(K_{DP})^{0.866} \text{ (mm h}^{-1}\text{)}, \tag{16}$$

in which KDP is in deg km^{-1}. Combining (16) with

$$Z_r = 200R^{1.6} \text{ (mm}^6 \text{ m}^{-3}\text{)}, \tag{17}$$

we obtain the following Z_r, K_{DP} relationship:

$$Z_r = 24800(K_{DP})^{1.386}. \tag{18}$$

Now the reflectivity factor of hail is estimated as

$$Z_h = Z - Z_r \text{ (mm}^6 \text{ m}^{-3}\text{)}. \tag{19}$$

Two limitations are associated with this estimate of hail reflectivity. First, the Z_r, R relationship (17) may not be appropriate for a particular rain–hail mixture, in which case an unknown bias will be present. Second, errors in Z and Z_r will cause errors in Z_h. These can be controlled because they depend on the number of samples M, Doppler spectrum width, and other known

or assumed parameters. From the statistical analysis in the Appendix it seems that quantifying hail with this simpler technique may be feasible as long as its reflectivity factor is at least 7 dB more than the reflectivity factor of rain in the mixture.

6. Radar observations

Two case studies of radar observations pertaining to mixed-phase precipitation on the ground are presented. The data were collected using the 10-cm, dual-polarization, NSSL radar at Cimarron. The quantification of rainfall and hailfall rate is based on the methodology described earlier.

a. Analysis of 14 May 1986 data

Severe thunderstorms on this day lasted longer than 24 hours across Oklahoma. These storms produced eight tornadoes, strong winds, hail, and flooding. Across many areas of the state hail ranging from ¾ to 4½ inches in diameter fell, accompanied by 3 to 4 inches of rain, in a few hours (NOAA Storm Data 1986). Radar data presented here are from vertical cross sections (RHI) over Norman when pea-sized hailstones mixed with rain were observed by NSSL scientists. The mixed-phase precipitation subsequently tapered off to nearly pure rain on the ground. Rawinsonde data showed that the 0°C isotherm on this day was at 3.5 km.

Two sample plots of the vertical profiles of Z, K_{DP}, and Z_{DR} are presented in Fig. 7. Here Z and Z_{DR} are averaged over 2.25 km in range. Using Eq. (7) K_{DP} is obtained over the same range interval. Data were collected about a range of 40 km, with the radar scanning in an RHI mode. The first plot is for the time when the mixed-phase precipitation was observed on the ground; Fig. 7b represents data from the decay stage of the storm when the hail fall ceased. The vertical profile of Z (Fig. 7a) shows that the reflectivities of 45 dBZ extend as high as 10 km, indicating a high probability of hail on the ground (Waldvogel et al. 1979). Absence of a distinctive melting layer in the Z profile is typical of convective storms. The K_{DP} rapidly increases below 3.6 km and thus one can infer the onset of melting. The differential reflectivity Z_{DR} increases slowly below the 0° isotherm. This could correspond to tumbling or spherical hail, also in conformity with the K_{DP} profile that is zero above 4 km. With the onset of melting, liquid water builds and, if ice particles are larger then 9 mm, small water drops are shed (Rasmussen et al. 1984) that may coalesce to produce larger drops. Also, smaller partially melted hail and snow aggregates retain oriented oblate shape before larger hailstones melt. As soon as there is a small amount of oblate wet (or melted) hydrometeors, K_{DP} begins to increase. However, Z_{DR} changes more gradually because it depends on the axis ratio and reflectivity combinations of both rain and hail being weighted more toward the axis ratio of higher reflectivity hailstones, whereas K_{DP} is not affected by the presence of hail.

At the onset of melting, Z_{DR} is dominated by contributions from hail and is insensitive to the few raindrops. As melting proceeds, more drops are generated and Z_{DR} begins to grow. Thus, there is a 1 km lag between the altitudes at which Z_{DR} and K_{DP} start to increase significantly. This lag would depend on the hail reflectivity and the rate at which water drops are formed. It should be noted that although the small negative excursions of K_{DP} above 6 km altitude are within the experimental accuracies of K_{DP} measurement, their consistency suggests the presence of vertically oriented hydrometeors.

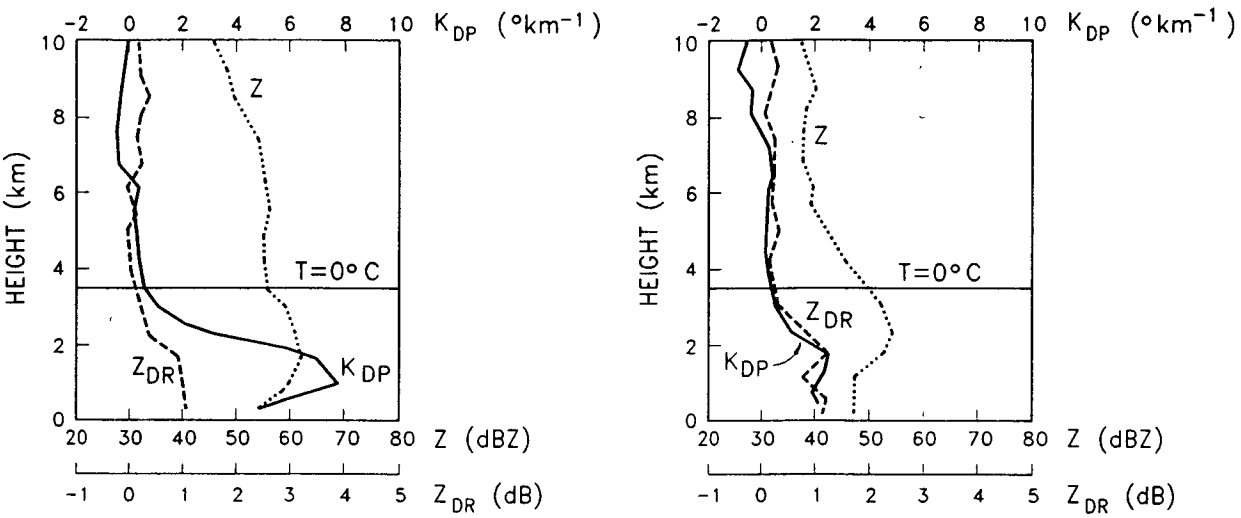

FIG. 7. Vertical profiles of Z, Z_{DR}, and K_{DP} at 1559:32 CST 14 May 1986. Range is 40 km and azimuth is 130°. (b) As in (a) but at 1611:06 CST.

Below the melting layer, K_{DP} has the same height dependent form as Z, which decreases at 1.8 km because of the increase in fall velocity that acts to decrease the drop concentration (Battan 1966). The decrease in Z and the steady slight increase in Z_{DR} suggest progression of melting down to the ground, a possibility confirmed by observation of hail and rain mixture at the ground.

Figure 7b shows the vertical profiles of Z, Z_{DR}, and K_{DP} at the tail end of the storm. The 45 dBZ reflectivity is at a lower altitude of about 4 km. There is no significant lag in altitudes at which Z_{DR} and K_{DP} start to increase, indicating a low concentration of hail aloft. A more pronounced peak in the Z profile, showing the effects of changes in fall velocity, and constant K_{DP} and Z_{DR} near ground characterize a very low rate of hailfall, if any, at the ground. Also, the vertical profiles of Z and Z_{DR} in Figs. 7a and 7b indicate the changeover from a mature convective to a decaying "rain out" phase of the storm (note the distinct peaks about 2 km in Fig. 7b) with graupel aloft which melts causing a rapid increase in fall speed. At the earlier time (Fig. 7a) small hail (1 cm) mixed with rain was observed on the ground. Later (Fig. 7b) no hail was observed.

The scatter of measured Z and K_{DP} stratified according to altitude is given in Fig. 8a for the first few minutes of the storm (from 1559:00 CST to 1605:00 CST). The mean Z and K_{DP} variation for pure rain (section 5) is shown by a dotted line. Remarkable similarity with theoretical curves (Fig. 5) suggests a progressively larger amount of hail in the mixture with height, with the result that between 3 and 4 km most of the hydrometeors are frozen. Figure 8b is a scatter plot of Z–K_{DP} later in time when pure rain was observed at the ground.

The variations of Z, K_{DP}, and Z_{DR} with time are presented in Fig. 9. Data are averaged from 0.1 to 1 km in altitude and smoothed over half-minute intervals for clarity. Note that the reflectivity factor drops by more than 15 dB (from more than 60 dBZ), whereas Z_{DR} decreases by less than 1 dB from an otherwise modest 2 dB. The initial small Z_{DR} but large Z and subsequent small decrease in Z_{DR} but large decrease in Z are an indication of transition from mixed-phase precipitation to rain.

Algorithms for rain rate based on Z_H or on Z_H and Z_{DR} often fail if applied to a mixture of rain and hail. This is illustrated in Fig. 10. The empirical relationship given by Ulbrich and Atlas (1984), which is applicable for exponential drop size distribution, is used for $R(Z, Z_{DR})$; the $R(Z)$ relationship is due to Marshall–Palmer (17); $R(K_{DP})$ is given by (16). The accumulated rain measured by a low-resolution rain gauge (not shown) follows nearly the variations of $R(Z)$. This is because the rain gauge measures total accumulation due to both rain and hail.

During the initial portion of the storm $R(Z, Z_{DR})$ predicts unusually high rain (>500 mm h^{-1}) and hence is not represented in Fig. 10. Its high predictions are due to bias introduced in Z and Z_{DR} by the presence of hail. From the measured values of Z and Z_{DR}, the contributions Z_r and Z_{DRr} due to rain are obtained using the measurements of K_{DP} and assuming a dry oblate spheroidal hail. The rain rate computed using Z_r and Z_{DRr} is included in Fig. 10. As anticipated, $R(Z)$ predicts higher rain rate than $R(K_{DP})$ initially. At the

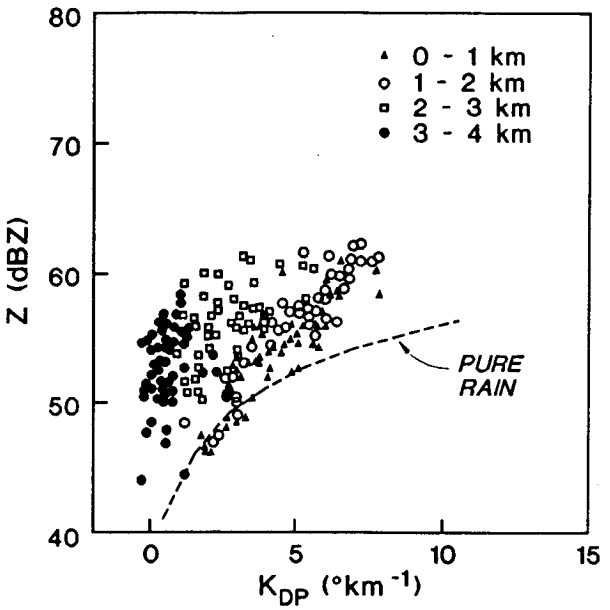

FIG. 8a. Scatterplots of Z and K_{DP} measured from 1559:00 CST to 1605:00 CST on 14 May 1986.

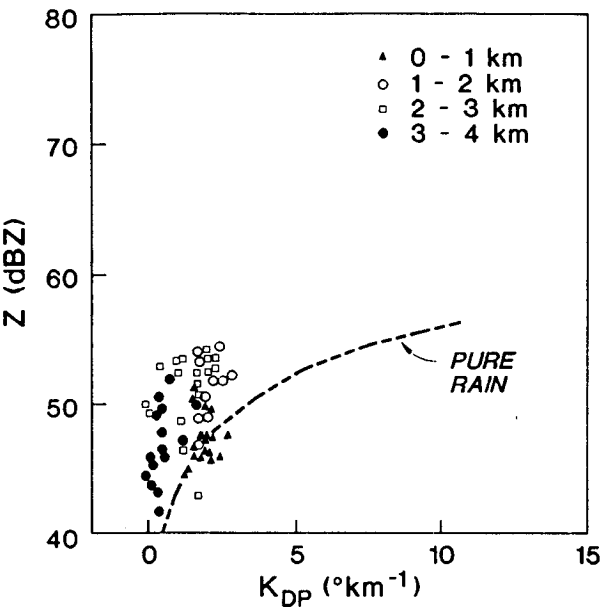

FIG. 8b. Scatterplots as in Fig. 8a, but from 1607:00 CST to 1612:08 CST.

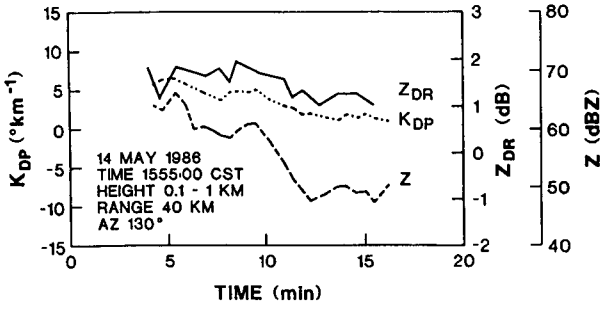

FIG. 9. Time history of Z, Z_{DR}, and K_{DP} produced by the storm on 14 May 1986.

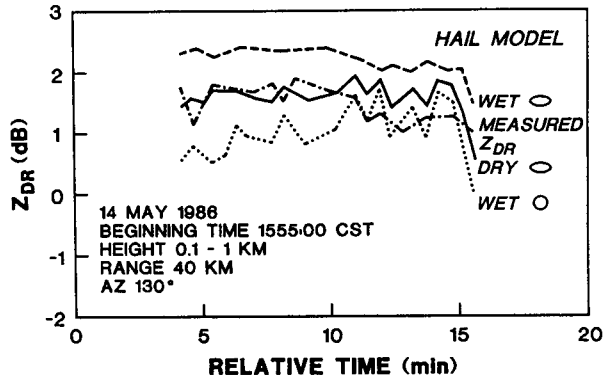

FIG. 11. Comparison of measured Z_{DR} with that predicted from measurements of Z and K_{DP} for a few models of hail.

tail end of the storm, $R(K_{DP})$ and $R(Z)$ are nearly equal, but $R(Z_r, Z_{DRr})$ is noisier and generally larger. This amply demonstrates that adequate caution must be exercised in using Z, Z_{DR} to predict rain rates in mixed-phase precipitation and that satisfactory correction is not always possible. We believe that the same reasons may explain the observation of Bumgarner and Dooley (1986) that in high reflectivity regions, algorithms based on Z_{DR} and Z, overestimate the rainfall rate. Both our model and observations imply that in mixed-phase precipitation, the actual rain rate is less than predicted by $R(Z)$, $R(Z, Z_{DR})$, or $R(K_{DP})$. However, the rain rate is closest to $R(K_{DP})$. A method of extracting actual hailfall rate and rainfall rate from the dual polarization data is described next.

Measured Z and K_{DP} are used to predict the Z_{DR} values for all the thermodynamic states and orientations of hail considered in section 3. The measured Z_{DR} and the predicted Z_{DR} (computed from measured Z and K_{DP}) for a few models are presented in Fig. 11. Most other models of hail produced large departures from the measured Z_{DR}, and hence are not included in Fig. 11. Considering only the initial portion of the storm, it is concluded from Fig. 11 that the hail seen in this storm is dry hail, oriented with the minor axes vertical. At about 11 min into data collection (Fig. 9), the Z drops below 50 dBZ, indicating a decrease in precipitation intensity. From there on the model of wet spherical hail agrees better, in an rms sense, with the measurements; the dry oblate hail model is biased with respect to the measurements, although it preserves a similar shape variation with time. The hailfall intensity during this time is very low, indicating that the dominant hailstones, if any, are smaller in diameter. Knight's measurements (Knight 1986) from other Oklahoma storms indicate that the axis ratios of smaller hailstones (<15 mm) are 0.9 or larger. This may explain our observation that, during the later part, the Z_{DR} measurement agrees well with that predicted using a wet spherical hail model.

Though the comparison of measured and predicted Z_{DR} is done for a variety of hail types and orientations (Fig. 11), in actual practice the vertical profiles of the polarimetric observables considerably reduce the comparisons to a manageably few models of hail. The hailfall and rainfall rates obtained from the measured Z, Z_{DR}, and K_{DP} are shown in Fig. 10. The rainfall rate is close to $R(K_{DP})$ for all practical purposes in this case, and hence is not shown separately. The negligible difference is due to the contribution to K_{DP} by oriented oblate hailstones.

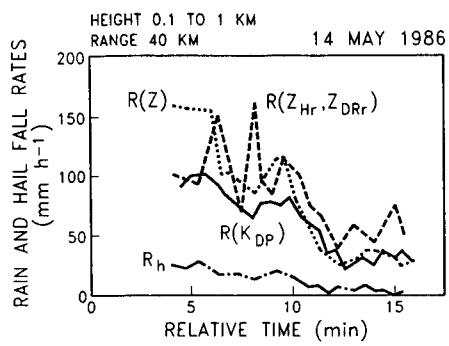

FIG. 10. Rain and hail rates versus time relative to 1555:00 CST.

b. *Analysis of 2 June 1985 data*

Severe weather on 2 June produced a series of tornadoes and stones varying in size from pea to baseball (NOAA Storm Data 1985). Some of the storms on this day produced radially aligned echoes behind strong reflectivity cores. Zrnić (1987) attributed this phenomenon to three-body scattering involving a path from large hail to the ground, from the ground back to the hail, and finally to the radar antenna.

The sounding on this day indicated a deep (surface to 800 mb) moist layer with a mixing ratio of >12 g kg^{-1} capped by an inversion. An almost dry adiabatic lapse rate of temperature extended from 750 to 500 mb to provide sufficient potential instability for strong updraft formation. The wind speed was increasing

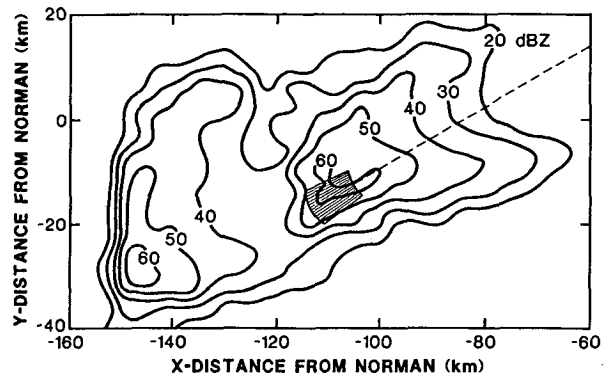

FIG. 12. Reflectivity factor Z_H contours measured with the Norman radar on 2 June at 1902:55; elevation angle is 0.4°. The location of the region where Cimarron data were collected is indicated, the dashed line is at 241° in azimuth from Cimarron.

throughout the troposphere, but with very little veering in the lowest levels. Thus, the environment was not conducive for supercell mesocyclonic storm formation but was very favorable for intense hailstorms.

Several RHIs were collected at successive azimuths and their location is superposed on the reflectivity factor contours, obtained by the Norman radar, in Fig 12. For every scan, 16 range gates were alternately positioned beginning at 82.5 and 87.15 km with a range resolution of 300 m; 512 alternately polarized samples were collected for each range and analyzed. This resulted in reduced altitude resolution compared with 14 May 1986 data (scan rates in elevation were the same), but improved accuracies in the radar estimates of Z, Z_{DR}, and K_{DP}.

Constant Z and Z_{DR} contours from elevation scans at two successive azimuths (241° and 242°) are given in Figs. 13a and 14a. The constant K_{DP} contours are presented in Figs. 13b and 14b. The K_{DP} contours are obtained by using a fifth-degree polynomial fit to ϕ_{DP} data from successive range gates and then taking the derivative with respect to range to reduce the edge effect and present this data over the same range as Z and Z_{DR}.

From Fig. 13a, we see that, between 82.5 and 85.5 km, Z_{DR} is negative and Z is close to 60 dBZ near the ground. This indicates the presence of hailstones oriented with their minor axes horizontal. Rawinsonde data on this day indicate that the 0°C isotherm was at 4.8 km height. An interesting observation is the relationship between Z, Z_{DR}, and K_{DP} signatures at points marked A to D in Fig. 13a near the ground. The reflectivity factor Z above points A, B, and C is larger

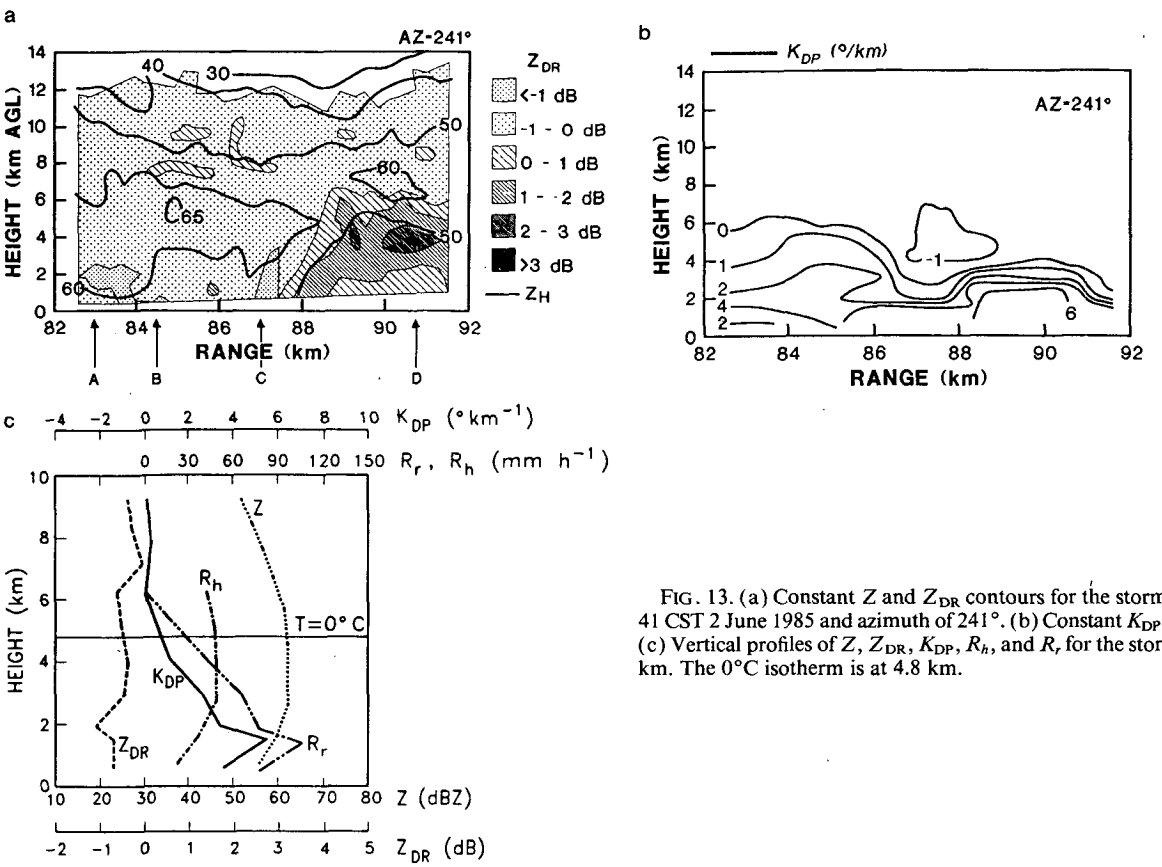

FIG. 13. (a) Constant Z and Z_{DR} contours for the storm at 1858: 41 CST 2 June 1985 and azimuth of 241°. (b) Constant K_{DP} contours. (c) Vertical profiles of Z, Z_{DR}, K_{DP}, R_h, and R_r for the storm at 84.5 km. The 0°C isotherm is at 4.8 km.

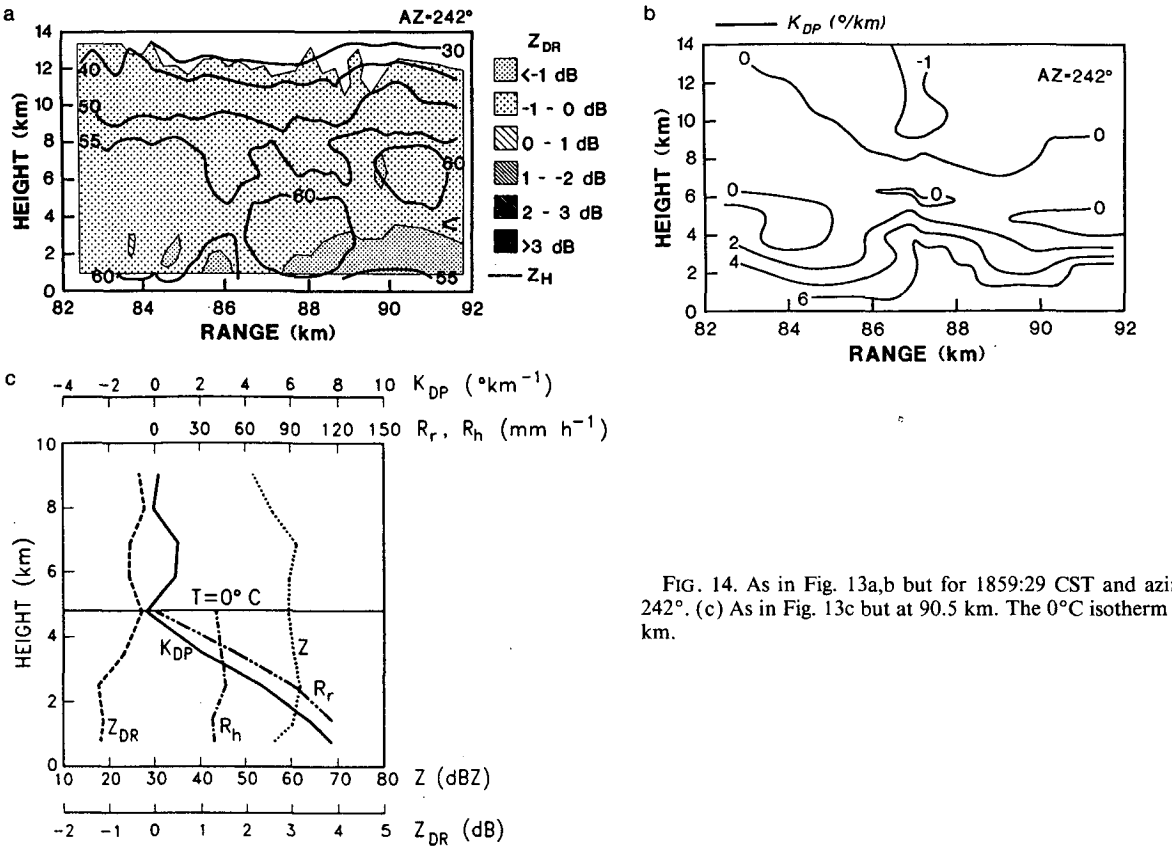

FIG. 14. As in Fig. 13a,b but for 1859:29 CST and azimuth of 242°. (c) As in Fig. 13c but at 90.5 km. The 0°C isotherm is at 4.8 km.

than 60 dBZ. At point A, Z_{DR} is less than −1 dB, and K_{DP} is 2° km^{-1}, whereas at point B Z_{DR} is larger than −1 dB, and K_{DP} is 4° km^{-1}. These signatures indicate (from Figs. 5a–d) that precipitation at A has a larger ratio of R_h/R_e than precipitation at B; also after examining K_{DP} data for heights above 5 km (Fig. 13b) we speculate that precipitation there is frozen, with the possible exception of small supercooled droplets. General features of the Z_{DR} and Z fields are similar to the observations by Bringi et al. (1986b) in a Colorado hail storm, except that our negative Z_{DR} values have larger magnitudes. The difference may be due to sizes that were smaller (≤3 cm) in the Colorado storm, compared with >4 cm in the Oklahoma storm. Knight (1986) presented evidence that larger hailstones are more oblate; if their minor axes are horizontally oriented they would, according to our model, produce larger $|Z_{DR}|$ than smaller hailstones.

Vertical profiles of Z, Z_{DR}, and K_{DP}, averaged over 2.1 km in range (centered at 84.5 km, point B), are given in Fig. 13c. The Z variations and height of the 45 kBZ level, above the 0°C isotherm, indicate a higher probability of hailfall. At the cloud top of 12 km Z_{DR} is nearly 0 dB. It decreases to −0.7 dB at 6 km. Around the 0°C isotherm (4.8 km), Z_{DR} is close to 0 dB; below, Z_{DR} decreases. Above the 0°C isotherm K_{DP} is small but positive, whereas at lower heights it increases.

Decreasing Z_{DR} and small but positive K_{DP} between 7 km and 6 km (Fig. 13c) could be reconciled by the graupel growth with ice crystals as embryos (Pruppacher and Klett 1978). Simultaneous presence of graupel and oriented hail could present negative Z_{DR} and small positive K_{DP} signatures. According to Knight and Knight (1970) and List (1959) the stable mode for small hailstones (<20 mm) is with a minor axis oriented vertically. Larger hailstones may fall with their minor axis horizontal. Without supporting evidence it is not possible to infer precisely the relative composition of hydrometeors above the freezing level. Another possibility is that, between 7 and 5 km, precipitation contains supercooled water drops brought up by the updraft, in addition to graupel and small hailstones. Although it is not possible to deny the presence of small droplets (not detectable by the radar), previous evidence (Wakimoto and Bringi 1988) has shown that signatures of large drops, extending on both sides of the melting layer, are visible as a positive Z_{DR} field, and disappear quickly because of freezing. We thus conclude that it is unlikely that significant amounts of supercooled drops are present in the region between 7

and 5 km. This is supported by our observation that K_{DP} is less than 0.5 deg km^{-1} in this region.

Below the 0°C isotherm, melting and shedding of water stabilize the orientation of hailstones, in this case, with their minor axes horizontal. Water drops contribute to the increase in K_{DP} seen below 0°C isotherm, similar to the May 14 case (Fig. 7a). The increase of K_{DP} confirms that the melting and shedding are incomplete even at the ground level; this is a characteristic of mixed-phase precipitation. We notice kinks in the vertical profiles of Z_{DR} and K_{DP} (Fig. 13c) near a 2 km height. From Figs. 13a and 13b it is seen that these have been caused by the spatial averaging (over 2.25 km centered at 84.5 km) of nonuniform K_{DP} (Fig. 13b) and Z_{DR} (Fig. 13a) at that level.

Comparison of data for 14 May 1986 (Fig. 7a) and for 2 June 1985 (Fig. 13c) shows that higher Z (>59 dBZ) and negative Z_{DR} are associated with the 2 June 1985 data. The cloud top height, as well as the subzero temperature region, are larger on 2 June. These also indicate that the hail size on 2 June is expected to be larger.

Values of Z and K_{DP} at heights less than 2 km (Fig. 13c) were used to predict Z_{DR} for dry, wet, and spongy hail (40% liquid water). In all cases the orientation of the hailstones is such that their minor axes are horizontal. Calculated and measured Z_{DR} were found to match closely when the spongy hail model was used. The rain- and hailfall rates using this model are given in Fig. 13c. The mixed-phase precipitation near the ground is seen to consist of 76 mm h^{-1} of rain and 23 mm h^{-1} of hail—$R_h/R_e \approx 0.24$. The precipitation rates in Fig. 13c assume that the liquid water content of the spongy hail is 40% at heights up to 4 km.

At point C (Fig. 13a) Z_{DR} is negative throughout, and only above point C negative K_{DP} values at 4–6 km heights are seen (Fig. 13b). Also the height at which K_{DP} begins to increase above zero is lower by more than 1 km from the 0°C isotherm. A hail shaft may be responsible for this descent of the 0° K_{DP} contour. If the precipitation were predominantly large hail, it could be oriented with minor axis horizontal and cause a small negative K_{DP}. Because thermal inertia of large hail is high, it would take some distance below the melting level before melting would produce measurable K_{DP}. This may be further aided (or alternately explained) if downward airflow is present, both by downward advection and by cooler air in which hailstones are imbedded.

The measurements at point D show a positive Z_{DR} column, otherwise the precipitation signature is similar to that seen in Fig. 7b, with a distinctive bright-band signature in both Z and Z_{DR}. The column and the one at 89 km may contain a low concentration of big raindrops mixed with spherical hail. Also, the reflectivity factor Z at point D is less than 55 dBZ near the ground.

RHI data collected over several azimuths on 2 June 1985 showed polarimetric signatures that are similar to those in Fig. 13. In some of the cross sections Z_{DR} is negative over the 10 km range, Z is 60 dBZ or larger, and the differential propagation phase shift (ϕ_{DP}) is more than 70°. These values indicate the severity and extent of the storm. The contour plots of Z and Z_{DR} measured at 242° azimuth are presented in Fig. 14a; Fig. 14b shows the constant K_{DP} contours. The signatures of Z, Z_{DR}, and K_{DP} around 86 and 90 km range (Figs. 14a and 14b) are similar to those seen near point C in Figs. 13a and 13b. The large region of substantial negative Z_{DR} values is remarkable. Furthermore, two distinct depressions of the K_{DP} contours (Fig. 14b) suggest that two hail shafts may be present.

Vertical profiles of Z, Z_{DR}, and K_{DP} averaged over 2.1 km centered at 90.5 km in range are given in Fig. 14c. Note that the variations of Z, Z_{DR}, and K_{DP} are similar to those seen in Fig. 13c, but the kinks near 2 km height are not present in Fig. 14c. This is because Z, Z_{DR} (Fig. 14a), and K_{DP} (Fig. 14b) do not change much in the range (89.45 to 91.55 km) over which the spatial averaging is done. Values of K_{DP} in excess of 6 deg km^{-1} close to the ground indicate that the rain rate is >100 mm h^{-1}. The electromagnetic scattering model with spongy hail (40% liquid water) is also found to yield a closer match between predicted and measured Z_{DR} at lower heights. The precipitation rates in Fig. 14c are based on this model. The negative Z_{DR} (0 to −0.5 dB) and positive K_{DP} (0 to 1 deg km^{-1}) in the height interval 5.5 to 7.5 km are noteworthy. Aligned hail mixed with drops or with graupel may be the cause but this could not be independently verified.

7. Conclusions

The identification of precipitation type as rain, hail, and rain–hail mixture is possible from reflectivity factor Z and differential propagation constant K_{DP} measurements. The K_{DP} yields a good estimate of liquid water in a rain–hail mixture, and it can be used together with differential reflectivity Z_{DR} and reflectivity factor Z to infer hail rate also. This is because K_{DP} is sensitive to anisotropic hydrometeors (rain); pure hail, which is nearly isotropic and has a small refractive index, is almost transparent to K_{DP}. But the hail rate cannot be estimated uniquely because of the uncertainty in size distribution. In this paper a single parameter distribution is used for modeling polarimetric signatures; thus theoretical results are exploratory and qualitative. Differential reflectivity Z_{DR} depends on the relative amounts of rain and hail, and hence is not suitable, by itself or in combination with Z, to gauge the amount of either rain or hail in the mixture. We have shown, using radar data, and confirmed on the ground that $R(Z, Z_{DR})$ predicts large rainfall rates (>500 mm h^{-1}) when the precipitation is a mixture of rain and hail. Yet with a proper account for the rain and hail, the

corrected precipitation rate $R(Z_r, Z_{DR_r})$ becomes consistent with other algorithms and ground truth.

Modeling shows that Z_{DR} is positive whenever hailstones are oriented with their minor axes vertical. It is negative only when minor axes are horizontally oriented. This and the fact that wetness of hailstones increases Z and the magnitude of Z_{DR} make it possible to qualitatively infer the full pattern and the phase state of the hail. Our conclusions are based on the self-consistency of Z, Z_{DR}, and K_{DP} data obtained from two Oklahoma storms and their spatial correlation that is in accord with the postulated behavior.

Acknowledgments. Discussions with R. Doviak, C. Ziegler, M. Sachidananda, and D. Burgess, and their perceptive suggestions, are gratefully acknowledged. The computer codes for the extended T-matrix method was given to the authors by V. N. Bringi and J. Vivekanandan, who together with V. Chandrasekar showed considerable interest in this work. Engineering staff, led by D. Sirmans, was responsible for making polarization measurements possible. M. Schmidt and C. Clark performed data collection. Ms. Carole Holder typed the manuscript, and Ms. Joan Kimpel prepared the graphics. Part of this research was supported by the Joint Systems Program Office for the Next Generation Weather Radar.

APPENDIX

Standard Error of Hail Reflectivity Factor

We examine the standard error of Z_h estimate (19). Assuming that a standard error should be less than a fraction α of the mean value, we write

$$\mathrm{VAR}(Z_h) = \mathrm{VAR}(Z) + \mathrm{VAR}(Z_r) \leq \alpha^2(Z - Z_r)^2. \quad \text{(A1)}$$

An approximate expression for the VAR(Z) from Doviak and Zrnić (1984, p. 99) is:

$$\mathrm{VAR}(Z) = Z^2/(2ML\sigma_{vn}\sqrt{\pi}), \quad \text{(A2)}$$

where the denominator represents the equivalent number of independent samples at the output of a square law detector. The reflectivities on the Cimarron radar are obtained from a logarithmic receiver (square law is also available but not calibrated) for which the variance is about 15% larger. Nevertheless we consider the square law because it yields the smallest possible error. Here M is the number of time-averaged samples (in the case of alternate polarizations it is also the number of sample pairs); L is the number of averages in range, and σ_{vn} is the normalized (to the unambiguous interval) Doppler spectrum width. The variance of Z_r is related to the variance of K_{DP} through (18) by

$$\mathrm{VAR}(Z_r) = 1.18 \times 10^9 \times (K_{DP})^{0.772} \cdot \mathrm{VAR}(K_{DP}), \quad \text{(A3)}$$

where K_{DP} is in deg km^{-1}. VAR(K_{DP}) is expressed in terms of variance of the differential propagation phase shift ϕ_{DP} by Eq. (9).

Sachidananda and Zrnić (1986) produced curves for the standard errors of ϕ_{DP}. These errors are not sensitive to the Doppler spectrum width and hence an approximate equation for $\sigma_\phi{}^2$ can be written as

$$\sigma_\phi \approx (5.4)/M \,(\mathrm{deg\ km^{-1}}). \quad \text{(A4)}$$

From (8) and (A4) the variance of K_{DP} becomes

$$\mathrm{VAR}(K_{DP}) = (5.4)^2/[M^2 \sum_i (r_i - r_0)^2]. \quad \text{(A5)}$$

A sequence of substitutions (A5) to (A3) to (A1) and (A2) to (A1) produces the inequality:

$$Z^2[1/(4\pi M^2 L^2 \sigma_{vn}) - \alpha^2] + \alpha^2 \cdot 4.96 \times 10^4 Z K_{DP}^{1.38} + 3.44 \cdot 6 \cdot 10^{10} K_{DP}^{0.772} / [M^2 L(L/2 + 1)(L + 1)\Delta r^2] - 1.54 \cdot 10^8 K_{DP}^{2.772} \leq 0, \quad \text{(A6)}$$

where Δr is separation between adjacent range gates in kilometers. For a fixed rain rate (or K_{DP}) one can subtract Z_r from Z in the equality (A6) and plot Z_h vs. M. This is illustrated in Figure A1 where $K_{DP} = 4°$ km^{-1} ($R = 68$ mm h^{-1}) and $\sigma_{vn} = 0.04$ (this would correspond to 1 m s^{-1} if the unambiguous velocity

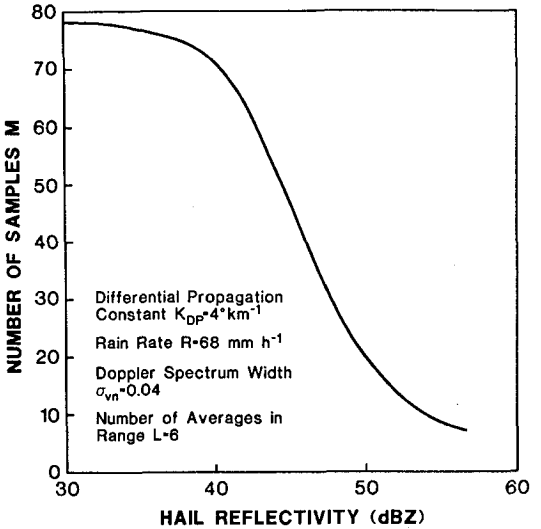

FIG. A1. Hail reflectivity Z_h and the number of sample pairs M for a 1 dB variation in the mean value of Z_h.

interval were 25 m s^{-1}; here this interval corresponds to twice the pulse repetition time because polarization is alternating). The L is set to 6, which for a NEXRAD-type radar would mean the average in range is taken over 1 km; that average is also the range interval for calculating K_{DP}; α is set at 0.25, implying less than 1 dB variation in the mean value. The reflectivity factor of rain for this example is 52 dBZ, and we see that a reasonable number of samples (<50) suffices to yield acceptable precision as long as the reflectivity of hail is larger than about 45 dBZ.

REFERENCES

Atlas, D., and F. H. Ludlam, 1961: Multiwavelength radar reflectivity of hailstorms. *Quart. J. Roy. Meteor. Soc.*, **87,** 523–534.

——, and C. W. Ulbrich, 1977: Path- and area-integrated rainfall measurements by microwave attenuation in the 1–3 cm band. *J. Appl. Meteor.*, **16,** 1622–1631.

Aydin, K., T. A. Seliga and V. Balaji, 1986: Remote sensing of hail with a dual linear polarization radar. *J. Climate Appl. Meteor.*, **25,** 1475–1484.

Barber, P., and C. Yeh, 1975: Scattering of electromagnetic waves by arbitrarily shaped dielectric bodies. *Appl. Opt.*, **14,** 2864–2872.

Barge, L. G., 1972: Hail detection with a polarization diversity radar, Stormy Weather Group Scientific Report, MW-71, McGill University, Canada.

Barge, B. L., and G. A. Isaac, 1973: The shape of Alberta hailstones, *J. Rech. Atmos.*, **7,** 11–20.

Battan, L. J., 1959: *Radar Meteorology.* University of Chicago Press, 161 pp.

Bringi, V. N., T. A. Seliga and K. Aydin, 1984: Hail detection with a differential reflectivity radar. *Science,* **225,** 1145–1147.

——, R. M. Rasmussen and J. Vivekanandan, 1986a: Multiparameter radar measurements in Colorado convective storms, Part I: Graupel melting studies. *J. Atmos. Sci.*, **43,** 2545–2563.

——, J. Vivekanandan and J. D. Tuttle, 1986b: Multiparameter radar measurements in Colorado convective storms, Part II: Hail detection studies. *J. Atmos. Sci.*, **43,** 2564–2577.

Browning, K. A., and J. G. D. Beimers, 1967: The oblateness of large hailstones. *J. Appl. Meteor.*, **6,** 1075–1081.

Bumgarner, W. C., and J. T. Dooley, 1986: Radar differential reflectivity measurements in an Oklahoma thunderstorm. Preprints, *23rd Conference on Radar Meteorology,* Snowmass, Colorado, Amer. Meteor. Soc., 125–128.

Carte, A. E., and G. Held, 1978: Variability of hailstorms on the South African plateau. *J. Appl. Meteorol.*, **17,** 365–373.

Chandrasekar, V., V. N. Bringi and P. J. Brockwell, 1986: Statistical properties of dual polarized radar signals. Preprints, *23rd Conference on Radar Meteorology,* Snowmass, Colorado, Amer. Meteor. Soc., 193–196.

Cheng, L., and M. English, 1983: A relationship between hailstone concentration and size. *J. Atmos. Sci.*, **40,** 204–213.

Douglas, R. H., 1964: Hail size distributions. Preprints, *11th Weather Radar Conference,* Boulder, Amer. Meteor. Soc., 146–149.

Doviak, R. J., and D. S. Zrnić, 1984: *Doppler Radar and Weather Observations,* Orlando, Academic Press, 458 p.

Eccles, P. J., and D. Atlas, 1973: A dual-wavelength radar hail detector. *J. Appl. Meteor.*, **12,** 847–854.

Green, A. W., 1975: An approximation for the shape of large raindrops. *J. Appl. Meteor.*, **14,** 1578–1583.

Jameson, A. R., 1983: Microphysical interpretation of multi-parameter radar measurements in rain, Part I: Interpretation of polarization measurements and estimation of raindrop shapes. *J. Atmos. Sci.*, **40,** 1792–1802.

——, 1985: Microphysical interpretation of multiparameter radar measurements in rain, Part III: Interpretation and measurements of differential phase shift between orthogonal linear polarizations. *J. Atmos. Sci.*, **42,** 607–614.

——, 1987: Relations among linear and circular polarization parameters measured in canted hydrometeors. *J. Atmos. Oceanic Technol.*, **4,** 634–645.

——, and R. C. Srivastava, 1978: Dual-wavelength Doppler radar observations of hail at vertical incidence. *J. Appl. Meteor.*, **17,** 1694–1703.

——, and E. A. Mueller, 1985: Estimation of propagation-differential phase shift from sequential orthogonal linear polarization radar measurements. *J. Atmos. Oceanic Technol.*, **2,** 133–137.

Knight, C. A., and N. C. Knight, 1970: The falling behavior of hailstones. *J. Atmos. Sci.*, **27,** 672–681.

Knight, N. C., 1986: Hailstone shape factor and its relation to radar interpretation of hail. *J. Climate Appl. Meteor.*, **25,** 1956–1958.

Leitao, M. J., and P. A. Watson, 1984: Application of dual linearly polarized radar data to prediction of microwave path attenuation at 10–30 GHz. *Radio Sci.*, **19,** 209–221.

List, R., 1959: Zur aerodynamik van hagelkornern. *Z. Angew. Math. Phys. 10,* 143–159.

Longtin, D. R., C. F. Bohren and L. J. Battan, 1987: Radar backscattering by large, spongy ice oblate spheroids. *J. Atmos. Oceanic Technol.*, **4,** 355–358.

Mason, B. J., 1971: *The Physics of Clouds.* Clarendon, 672 pp.

Matson, R. J., and A. W. Huggins, 1980: The direct measurement of the sizes, shapes and kinematics of falling hailstones. *J. Atmos. Sci.*, **37,** 1107–1125.

McCormick, C. G., and A. Hendry, 1975: Principles for the radar determination of the polarization properties of precipitation, *Radio Sci.*, **10,** pp. 421–434.

——, and ——, 1979: Techniques for the determination of the polarization properties of precipitation. *Radio Sci.*, **14,** pp. 1027–1040.

McGuinness, R., and A. Holt, 1989: The extraction of rain rates from CDR data. Preprints, *24th Conference on Radar Meteorology,* Tallahassee, Amer. Meteor. Soc., 338–341.

Metcalf, J. I., 1986: Interpretation of autocovariances and cross covariances from a polarization diversity radar. *J. Atmos. Sci.*, **43,** 2479–2498.

Mueller, G. A., 1984: Calculation procedure for differential propagation phase shift. Preprints, *22nd Conference on Radar Meteorology,* Zurich, Amer. Meteor. Soc., 397–399.

NOAA Storm Data, 1985: Vol. 27, National Climatic Data Center, Asheville, June, 70 pp.

——, 1986: Vol. 28, National Climatic Data Center, Asheville, May, 46 pp.

Oguchi, T., 1983: Electromagnetic propagation and scattering in rain and other hydrometeors. *Proc. IEEE,* **71,** 1929–1078.

Pruppacher, H. R., and J. D. Klett, 1978: *Microphysics of Clouds and Precipitation.* Reidel, 714 pp.

Rasmussen, R. M., V. Levizzani and H. R. Pruppacher, 1984: A wind tunnel and theoretical study on the melting behavior of atmospheric ice particles: III. Experiment and theory for spherical ice particles of radius > 500 μm. *J. Atmos. Sci.*, **41,** 381–388.

Rinehart, R. E., and J. D. Tuttle, 1984: Dual-wavelength processing: Some effects of mismatched antenna beam patterns. *Radio Sci.*, **19,** 123–131.

Sachidananda, M., and D. S. Zrnić, 1986: Differential propagation phase shift and rainfall rate estimation. *Radio Sci.*, **21,** 235–247.

——, and ——, 1987: Rain rate estimated from differential polarization measurements. *J. Atmos. Oceanic Technol.*, **4,** 588–598.

——, and ——, 1989: Efficient processing of alternately polarized radar signals. *J. Atmos. Oceanic Technol.*, **6,** 173–181.

Seliga, T. A., and V. N. Bringi, 1976: Potential use of radar reflectivity at orthogonal polarizations for measuring precipitation. *J. Appl. Meteor.*, **15,** 69–76.

Sirmans, D., and J. T. Dooley, 1986: A numerical comparison of three differential reflectivity estimates. Preprints, *23rd Conference on Radar Meteorology,* Snowmass, Colorado, Amer. Meteor. Soc., 189–192.

Steinhorn, I., and D. S. Zrnić, 1988: Potential uses of differential propagation phase constant to estimate raindrop and hailstone size distributions. *IEEE Trans. Geosci. Remote Sens.,* **26,** 639–648.

Torlaschi, E., R. G. Humphries and B. L. Barge, 1984: Circular polarization for precipitation measurement. *Radio Sci.,* **19,** 193–200.

Tuttle, J. D., V. N. Bringi, H. D. Orville and F. J. Kopp, 1989: Multiparameter radar study of a microburst: Comparison with model results. *J. Atmos. Sci.,* **46,** 601–620.

Ulbrich, W. C., and D. Atlas, 1982: Hail parameter relations: A comprehensive digest, *J. Appl. Meteor.,* **21,** 22–43.

——, and ——, 1984: Assessment of contribution of differential polarization to improved rainfall measurements, *Radio Sci.,* **19,** 49–57.

Wakimoto, R. M., and V. N. Bringi, 1988: Dual-polarization observations of microbursts associated with intense convection: The 20 July storm during the MIST project. *Mon. Wea. Rev.,* **116,** 1521–1539.

Waldvogel, A., B. Federer and P. Grimm, 1979: Criteria for the detection of hail cells. *J. Appl. Meteor.,* **18,** 1521–1525.

Warner, C., 1978: Calculated scattering characteristics of hailstones at weather radar wavelengths. Alberta Research Council, Rep., 24 pp.

Ziegler, C. L., P. S. Ray and N. C. Knight, 1983: Hail growth in an Oklahoma multicell storm. *J. Atmos. Sci.,* **40,** 1768–1791.

Zrnić, D. S., 1987: Three-body scattering produces precipitation signature of special diagnostic value. *Radio Sci.,* **22,** 76–86.